LIMNOLOGY
and
OCEANOGRAPHY

ASLO

Limnol. Oceanogr. 61, 2016, 2191–2206

doi: 10.1002/lno.10365

Thermodynamics and hydrodynamics in an atoll reef system and their influence on coral cover

Justin S. Rogers,*[1] Stephen G. Monismith,[1] David A. Koweek,[2] Walter I. Torres,[1] Robert B. Dunbar[2]
[1]Environmental Fluid Mechanics Laboratory, Stanford University, Stanford, California
[2]Department of Earth System Science, Stanford University, Stanford, California

Abstract

We present results of the thermodynamics and hydrodynamics of an atoll system and their effect on coral cover based on field measurements from 2012 to 2014 on Palmyra Atoll in the central Pacific. We found that spatial variations in coral cover were correlated with temperature variations on time scales of days to weeks. Shallow terrace and backreef sites with high coral cover (> 50%) had a highly variable temperature distributions, but their average weekly temperature distributions were lower and similar to offshore waters. The mechanism for maintaining this low weekly temperature was mean advection, which varied on a weekly timescale in response to wave forcing. Tides were also important in driving flow on the atoll, but their contribution to the net transport of heat was not significant. Wind and regional forcing were generally not important in driving flow inside the atoll. Buoyancy-driven flows were important within the lagoons, and in driving cross-shore exchange on forereef environments. The physical factors favoring high coral cover percentage varied according to the different prevailing hydrodynamic regimes: low temperatures in backreef habitats, short travel times in lagoon habitats (days since entering the reef system), and lower wave stress on forereef habitats. In light of future warming from climate change, local areas of reefs which maintain lower temperatures through wave-driven mean flows will have the best likelihood of promoting coral survival.

Globally, reef building corals face elevated extinction risk from climate change (Carpenter et al. 2008). Reef-building corals have experienced global declines resulting from bleaching events caused by week to month-long warm-water exposure (Hughes et al. 2003; Hoegh-Guldberg et al. 2007; Carpenter et al. 2008). However, corals in naturally warm environments can exhibit enhanced resistance to bleaching at high temperatures up to some limiting threshold, and studies show evidence of both short-term acclimatory and longer-term adaptive acquisition of climate resistance (Palumbi et al. 2014). Corals can often resist high temperature variability at hourly time scales (Mayfield et al. 2013; Dandan et al. 2015), but may be more vulnerable to disease and even experience mortality when exposed to elevated temperatures at time scales of several days to weeks (Bruno et al. 2007; Williams et al. 2010; Palumbi et al. 2014). Thus, in light of global climate change, understanding local thermal variability on reefs is important.

*Correspondence: jsrogers@stanford.edu

Additional Supporting Information may be found in the online version of this article.

Reef thermal variability (i.e., spatial and temporal deviations from offshore conditions) can be driven by atmospheric forcing (e.g., solar radiation, wind, and surface heat fluxes) (Smith 2001; Wells et al. 2012; Zhang et al. 2013), as well as from advection driven by waves, tides and other forcing (Davis et al. 2011; Herdman et al. 2015). While diurnal temperature variability can be quite high on shallow back reefs (Herdman et al. 2015), the longer term weekly or monthly averaged temperatures appear to be more stressful to corals (Williams et al. 2010; Palumbi et al. 2014). These long-term temperatures are the basis for time integrating reef bleaching predictors such as the degree heating week, which is a cumulative measure of thermal stress (Strong et al. 2011). Little work, however, has been done to relate weekly temperature variability to observed benthic community composition in a mechanistic manner.

Thermodynamics on coral reefs are strongly influenced by the physical transport of sea water, and thus quantifying the distribution and variability of temperature requires a mechanistic understanding of the hydrodynamic forces driving reef circulation; for example, waves, tides, regional flow, wind, and buoyancy effects. These mechanisms have different importance depending on the length scale of interest (Monismith 2007). Waves have long been recognized as the

dominant forcing mechanism driving circulation and transport on many reefs (Munk and Sargent 1948; Symonds et al. 1995; Kraines et al. 1998; Lugo-Fernández et al. 2004; Callaghan et al. 2006; Lowe et al. 2009). However, while about two-thirds of reefs globally are wave dominated, the remaining one-third are tidally dominated (Lowe and Falter 2015).

The classic dynamical basis by which waves drive flow is by changes to the waves from physical processes such as shoaling, refraction, dissipation, and so forth, which create spatial gradients in radiation stresses and impart a force in the momentum equation (Longuet-Higgins and Stewart 1964). Conceptually, wave dissipation from breaking or bottom friction increases the mean water level, known as wave setup, establishing a pressure gradient that drives flow across the reef in the direction of wave propagation (Munk and Sargent 1948; Young 1989; Lowe et al. 2009). On reefs, wave dissipation by bottom friction can be quite high due to the complex bathymetry (Monismith et al. 2015; Rogers et al. 2016), and physically, this can create less wave breaking and lower setup; thus reducing the strength of circulation.

In addition to being driven by waves, circulation can be driven by tides, regional flows, winds, and buoyancy effects. Tides can generate circulation in larger and more enclosed lagoons where the channels connecting the lagoon with the open ocean are relatively narrow, and the constricted exchange of water between these lagoons and the open ocean can cause significant phase lags between lagoon and offshore water levels (e.g., Dumas et al. 2012; Lowe and Falter 2015). Large-scale oceanographic features such as eddies and currents as well as island-scale features such as the vortices shed by seamounts and headlands can also be important in driving local patterns of reef circulation (Arístegui et al. 1994; Wolanski et al. 1996; Monismith 2007). Wind stresses often play only a minor role in driving the circulation of shallow reefs; however, wind forcing can be important or even dominant in the circulation of deeper and more isolated lagoons (Atkinson et al. 1981; Delesalle and Sournia 1992; Douillet et al. 2001; Lowe et al. 2009). Finally, buoyancy forcing can drive reef circulation through either temperature- or salinity-driven stratification in certain reef systems (Monismith et al. 2006; Hoeke et al. 2013; Herdman et al. 2015). The flow accelerated by these forcing mechanisms is resisted by bottom friction, which can be quite high on some reefs due to complex bathymetry (Rosman and Hench 2011; Rogers 2015).

Atolls represent a geologic end-member for reefs, and are a common feature throughout the world's tropical oceans (Riegl and Dodge 2008). Atoll geomorphology includes exterior reefs and terraces exposed to oceanic flows and an interior lagoon system separated by a reef crest and reef flat with connecting channel systems. These separate yet interconnected hydrodynamic regimes are a feature that differs from fringing and barrier reefs. Previous studies have focused on specific aspects of atoll systems (Kench 1998; Andréfouët et al. 2006; Dumas et al. 2012), but to our knowledge no studies have yet examined the circulation and thermodynamics of an atoll system holistically. The lack of atoll-wide thermal and hydrodynamic studies inhibits our ability to understand coral reef ecosystem function and how the circulation patterns within atolls may ameliorate or inhibit the multitude of stressors affecting coral reefs, beyond just thermal stress.

Palmyra Atoll is part of the Northern Line Islands in the central equatorial Pacific and provides an excellent natural laboratory in which to investigate coral reefs in the absence of acute anthropogenic stressors due to its relative isolation from direct human impact (Stevenson et al. 2007; Sandin et al. 2008; Williams et al. 2013). To our knowledge, there have been no studies of reef circulation and thermodynamics done in any of the Line Islands including Palmyra; and previous studies have relied on using results from remote sensing (e.g., sea surface temperature, Chlorophyll *a*) or regional climate models (e.g., global Wave Wave 3 model) which have not been locally validated (Riegl and Dodge 2008; Williams et al. 2013; Gove et al. 2015; Stevenson et al. 2015). The lack of local, long-term hydrodynamic measurements in the central equatorial Pacific, remains a serious knowledge gap in our understanding of coral reef ecosystems in this region and; thus, limits our ability to predict the fate of these reefs in a future subject to increased warming, acidification, and otherwise changing climate.

While the hydrodynamic forcing and thermodynamics on fringing and barrier reef systems have already been well investigated (Lowe and Falter 2015), little work has been done to examine how variability to the oceanic forces driving circulation and the atmospheric forces driving net heat fluxes on open atolls affect spatial and temporal patterns in atoll temperatures; let alone how well the resulting hydrodynamics and thermodynamics can explain spatial patterns in coral cover. The aim of this study is to address this knowledge gap using field measurements of waves, circulation and temperature on Palmyra Atoll from 2012 to 2014. We then investigate the effects of different forcing mechanisms in driving flow and temperature variability, and address the role of temperature in shaping the ecological community structure of Palmyra.

Study site and methods

Study site

Palmyra Atoll (5° 52′N, 162° 05′W) is part of the Northern Line Islands of the central equatorial Pacific (Fig. 1a). Largely because of the absence of acute anthropogenic stressors, Palmyra's exposed reef tracts (outside of the lagoons) contain abundant and diverse calcifiers, namely hard corals and crustose coralline algae (Williams et al. 2013) with relatively high community production and calcification rates (Koweek

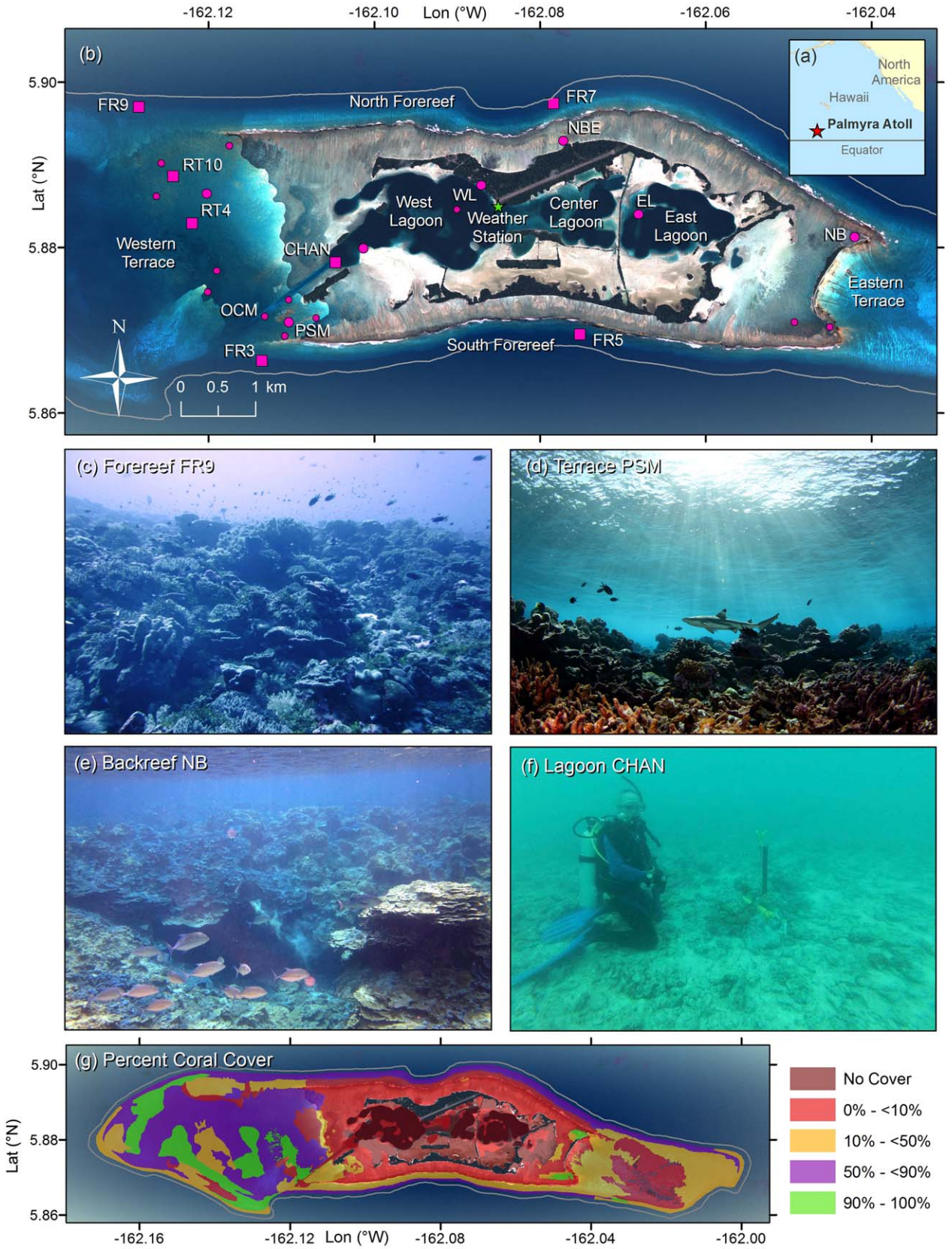

Fig. 1. Palmyra Atoll location, site layout and experiment instrumentation. (**a**) location of Palmyra Atoll, (**b**) layout of atoll and instrument locations for long term measurement [(U, ζ, T) magenta squares; (ζ, T) magenta circles; (T) small magenta circles), and weather station (green star), image courtesy of NOAA. (**c**) typical northern forereef near FR9 with abundant live coral and fish, (**d**) typical terrace with blacktip shark (*Carcharhinus limbatus*) near PSM courtesy of Brian Zgliczynski, (**e**) typical shallow back reef with live coral near NB, (**f**) typical lagoon rubble bottom with low visibility water near CHAN with diver and ADV for scale, and (**g**) percent coral cover mapping courtesy of NOAA. Gray line on (b,g) is 100-m depth contour.

et al. 2015). The atoll consists of a forereef, reef crest and shallow back reef region on both its northern and southern sides with open terraces supporting high coral cover typically greater than 50% at depths of 5 m to 20 m dominating the western and eastern edges (Fig. 1b–g). The percent coral cover was obtained from National Oceanic and Atmospheric Administration (NOAA) National Center for Coastal Ocean Science Benthic Habitat Mapping [http://products.coastalscience.noaa.gov/collections/benthic/e58palmyra/] (Fig. 1g). The forereefs are characterized by high (> 50%) percentages of live hard coral cover (Fig. 1c). In the surfzone, the substrate largely consists of rubble whereas further inshore of the reef crest, larger corals are common on the back reef (Fig. 1d). The terraces are typically characterized by high coral cover (> 50%), high rugosity, and complex bathymetry while lagoonal areas typically exhibit seabeds of sediment (Fig. 1e,f) (Williams et al. 2013). The interior lagoons were significantly modified and constricted during World War II (Collen et al. 2009), and are typically strongly stratified with anoxic and sulphidic bottom waters (Gardner et al. 2014).

Field experiment

The field experiment consisted of an array of velocity and pressure sensors deployed between September 2012 and July 2014 designed to characterize the waves and hydrodynamics around the atoll (Fig. 1b, Supporting Information Table SI 1). The wave dynamics of the atoll have already been described by Rogers (2015), Rogers et al. (2015), and Monismith et al. (2015). Pressure measurements were made with Richard Brancker Research DR1050 and Virtuoso sensors; velocity and pressure measurements were made with RDI Teledyne Acoustic Doppler Current Profilers (ADCPs), Nortek Acoustic Doppler Profilers (ADPs), and Nortek Acoustic Doppler Velocimeters (ADVs); salinity was inferred from Sea-Bird Electronics SBE-37 Conductivity Temperature Depth sensors; and temperature measurements were made with Sea-Bird Electronics SBE-56 thermistors and SBE-37s (Supporting Information Table SI 1). Note that battery power constrained sampling frequencies for long-term experiments due to the long times (ca., 1 yr) between instrument deployment and recovery. Monitoring stations with ADCPs or ADPs attached to polyethylene plates were secured to the reef in areas of dead coral or sand. Monitoring stations with only a pressure and/or temperature sensors were secured directly to dead corals on the reef substrate. Most of the sites were outfitted with a single bottom mounted thermistor, but at the forereef sites (FR3, FR5, FR7, FR9) bottom mounted thermistors were placed at 10-m, 20-m, and 30-m depth, and vertical moorings were placed at the channel inlet and outlet (CHAN and OCM, 3 SBE56s each) and within the west lagoon (WL, 5-SBE56s).

Data analysis

Instantaneous measurements of velocity data were taken in (x, y, z) coordinates, with x and y corresponding to geographic east and north, respectively, and the vertical (z) coordinate is taken as upwards from mean sea level (MSL). The instantaneous field measurements were time-averaged (30 min) and interpolated to a common time to give Eulerian velocity $\boldsymbol{u_E}(u_E, v_E, w_E)$, free surface deviation from MSL ζ, temperature T, salinity S, and wave statistics. The mean Lagrangian velocity $\boldsymbol{u}$ was calculated by $\boldsymbol{u}=\boldsymbol{u_E}+\boldsymbol{u_S}$ (Andrews and Mcintyre 1978), where $\boldsymbol{u_S}$ is the Stokes drift computed spectrally from the wave data (Dean and Dalrymple 1991). Details of wave computations of significant wave height H_s, and other wave properties are discussed in Rogers et al. (2015). The Lagrangian depth-averaged mean velocity $\boldsymbol{U}$ (U, V, W) was calculated by combining available data at a given location (ADV/ADCP/ADP), assuming $\boldsymbol{u_E}=0$ at the bottom, linearly interpolating in z and taking the average. For some portions of the analysis, mean velocities were rotated into a cross-shore (CS) and alongshore (AS) components, that is, (u_{CS}, u_{AS}) and (U_{CS}, U_{AS}), with positive CS coordinate defined as toward the atoll center, and AS coordinate defined using the right-hand convention (i.e., positive AS on the north and south sides of the atoll is roughly west, and east, respectively). Notation for a 36-h low pass filter $(_{lp})$ and time averaging overline $(\bar{})$ is used consistently throughout.

The squared coherency γ^2 (Coh) between two signals is given by,

$$\gamma^2(f)=|S_{12}(f)|^2/S_{11}(f)S_{22}(f), \quad (1)$$

where $S_{ij}(f)$ is the cospectra of signal i with signal j as a function of frequency f. The limiting value for 95% confidence, $\gamma^2_{95}=1-0.05^{[1/(EDOF-1)]}$, where EDOF is number of independent realizations, and to effectively use coherency in a linear system, each of the inputs must not be coherent with each other (Emery and Thomson 2004).

Some wave and hydrodynamic modeling results from Rogers et al. (2015) and Rogers (2015) were included in this study. In brief, the model used the Coupled Ocean Atmosphere Wave Sediment Transport modeling system (Warner et al. 2010), to couple the Regional Ocean Modeling System (ROMS) hydrodynamic model with the Simulating Waves in the Nearshore (SWAN) wave model on a 50-m grid to compute water travel times throughout the Palmyra reef complex based on the movement of numerical Lagrangian passive drifters. Boundary conditions were based on the global Hybrid Coordinate Ocean Model (HYCOM).

Results

Oceanographic forcing

Wave height H_s varied seasonally with the highest waves being incident to the northern side of the atoll during winter in the northern hemisphere (up to 3.2 m) and to the southern side during summer in the northern hemisphere (up to 2.2 m) (Fig. 2a) (Rogers et al. 2016). The free surface ζ on the forereef varied primarily with tidal fluctuations of up

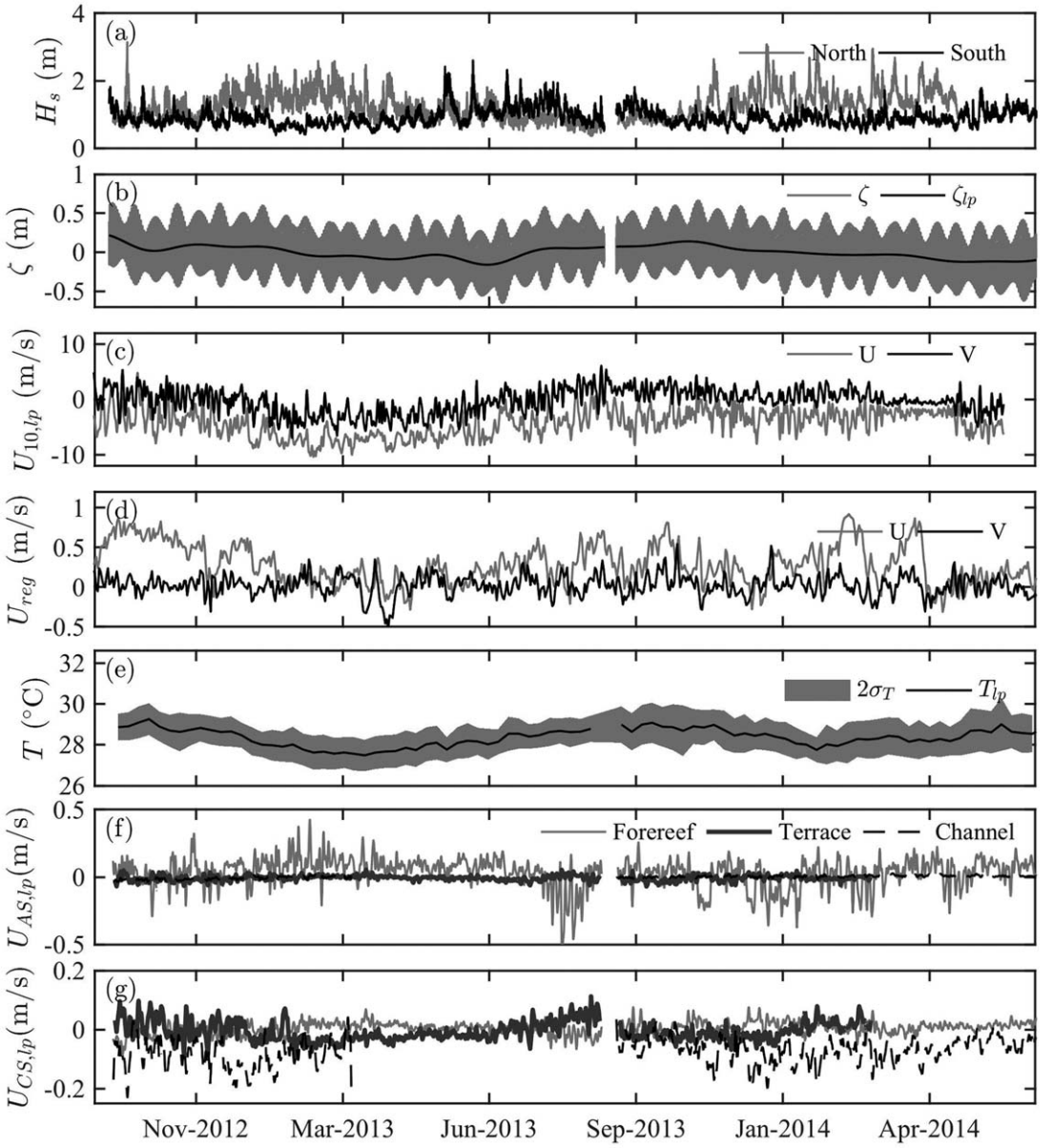

Fig. 2. Oceanographic field measurements, Sept 2012 to July 2014. (**a**) measured significant wave height H_s at north and south forereef, (**b**) forereef free surface height ζ and low pass filtered surface ζ_{lp}, (**c**) low pass filtered wind velocity $U_{10,lp}$ (oceanographic convention), (**d**) regional currents U_{reg} from upper 50 m of daily HYCOM model, (**e**) average low pass filtered temperature T_{lp} and standard deviation σ_T of all measurements, (**f**) measured low pass filtered depth averaged AS velocity $U_{AS,lp}$, and (**g**) measured low-pass filtered depth averaged CS velocity $U_{CS,lp}$. Positive CS coordinate is toward atoll center. Low pass filter (lp) is 36 h. For (f,g) forereef is FR9, terrace is RT4, channel is CHAN sites.

to 0.8 m, but also with long-term sea level fluctuations ζ_{lp} of 0.2 m (Fig. 2b). The winds on the atoll were dominated by the trade winds for much of the year (Maragos et al. 2008) and were directed primarily from the northeast and southeast directions with speeds up to 12 m s^{-1} $U_{10,lp}$ (Fig. 2c). The atoll is generally within the North Equatorial Counter Current (NECC), which flowed primarily to the east at typically 0.2 to 0.8 m s^{-1} from August to January, and was weak the rest of the year (< 0.2 m s^{-1}) (Maragos et al. 2008; Hsin and Qiu 2012). The regional currents derived from the daily average of the upper 50 m in the vicinity of Palmyra from the global HYCOM model showed generally easterly flows up to 0.8 m s^{-1}, which were strongest in the northern hemisphere winter consistent with the NECC (Fig. 2d).

Mean low-pass filtered temperature T_{lp} across all instruments varied during the 2-yr period by about 1°C, with 95% of measurements [2 standard deviations (σ_T) spatially and temporally] typically within 1°C of the mean (Fig. 2e). The AS depth averaged velocities U_{AS} were largest on the forereef, up to 0.6 m s^{-1} (Fig. 2f), and weaker in the CS direction

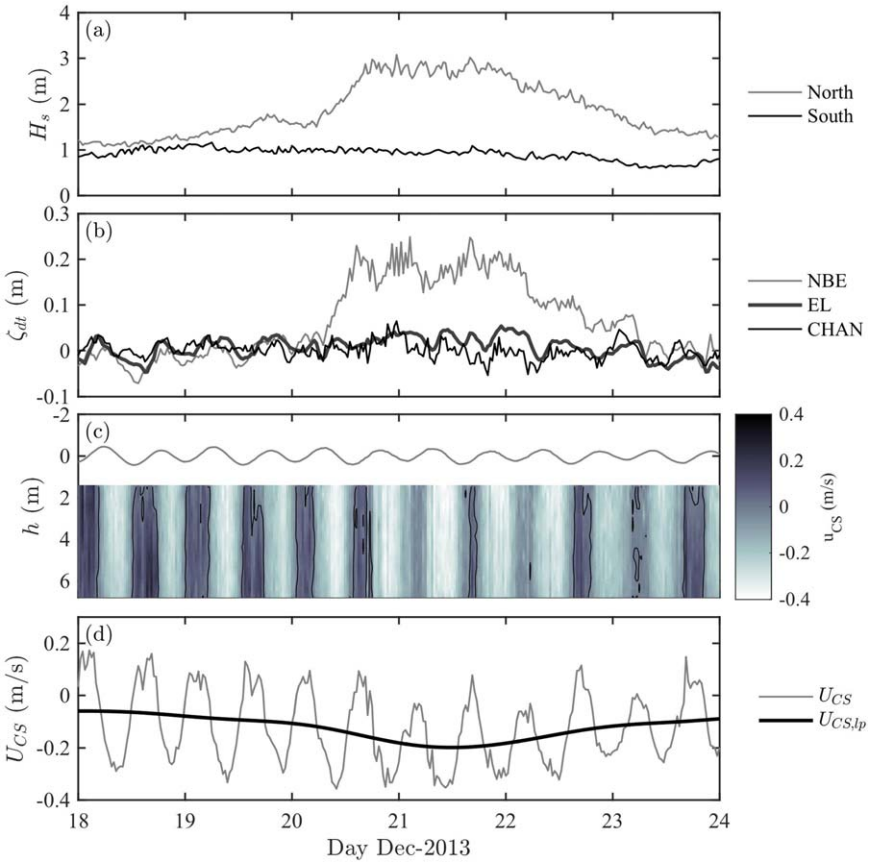

Fig. 3. Wave-driven flow through lagoon system measured in the channel, Dec 2013. (**a**) significant wave height H_s at north and south sides of atoll, (**b**) tidally removed free surface ζ_{dt} at north back reef (NBE), eastern lagoon (EL), and channel (CHAN), (**c**) free surface (gray) and along-channel velocity u_{CS} with depth at channel, zero velocity is black contour, (**d**) depth averaged velocity U_{CS} and 36-h low pass filtered velocity $U_{CS,lp}$ at channel. Positive velocity is oriented toward the lagoon. [Color figure can be viewed at wileyonlinelibrary.com]

where maximum U_{CS} of up to 0.2 m s^{-1} was observed on the terraces (Fig. 2g). The current ellipses show flow was generally aligned with bathymetric contours, except on the terrace; and the contribution of the M2 tide to flow was relatively small on the forereef (< 20% of overall velocity) while on the western terrace and channel the contribution was large (> 50% of overall velocity) (Supporting Information Figure SI 1b). The net mean flow over the measurement period was to the west on the south forereef, out of the lagoon in the channel, near zero on the western terrace, and to the east on the north forereef (Supporting Information Figure SI 1b). The free surface tidal amplitude was only slightly reduced with propagation into the lagoon system, but was significantly delayed by up to 4.3 h in the interior East Lagoon due to the constricted inlets (Supporting Information Figure SI 1a).

The reef on the atoll is in some areas very rough and rugose (Fig. 1), and previous field experiments have indicated very high wave friction factor f_w values between 0.5 and 5 (Monismith et al. 2015; Rogers et al. 2016). We used an empirical orthogonal function analysis on the measured velocity profiles at each site (*see* Supporting Information), and at most of the sites, the deeper part of the profile was roughly linear, indicating a log-layer like flow (Supporting Information Figure SI 2). Near the surface on the forereef and channel sites, the profiles deviated from the linear profile. Over all the sites, using logarithmic fit to the observed velocity profiles (*see* Supporting Information), the apparent roughness height z_{0a} including the effects of waves varied from 1.2 cm to 5.5 cm, and the physical roughness height z_0, (removing the effects of waves where applicable), varied from 0.17 cm to 3.7 cm (Supporting Information Table SI 2). Results for bottom drag coefficient C_D using Reynolds stress varied from 0.0037 to 0.10 (Supporting Information Table SI 2). These results for z_0 and C_D are consistent with the wide range of values observed on other reefs (Rosman and Hench 2011; Lentz et al. 2016).

Circulation

Flow on reefs strongly controls thermal variability and is governed by the depth integrated momentum equations for Lagrangian horizontal flow given by (e.g., Mei et al. 2005),

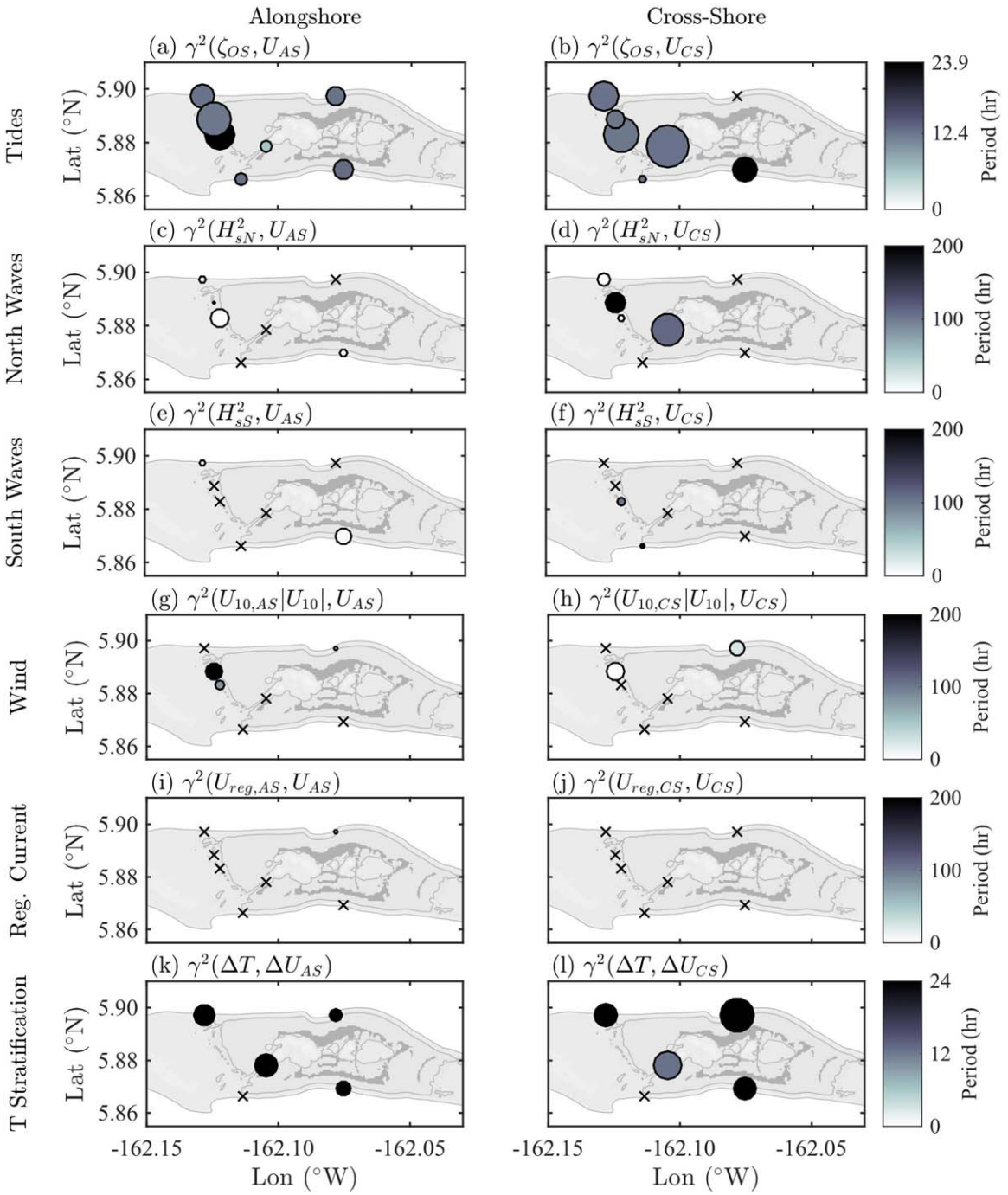

Fig. 4. Relative strength of forcing mechanisms in driving flow in AS (left) and CS (right) directions. Coherency between depth averaged flow *U* and forcing from (**a**,**b**) tides, (**c**,**d**) north waves, (**e**,**f**) south waves, (**g**,**h**) wind. (**i**,**j**) regional current. (**k**,**l**) Coherency between exchange flow ΔU and temperature stratification ΔT. Size of markers represent maximum squared coherency over all frequencies with largest marker in plot (a) equal to 0.98, and smallest marker equal to 95% significance (0.18). Values below 95% significance are black x. Shading represent period of maximum coherency. Light gray lines are 5- and 60-m depth contours, and light gray shading is land. [Color figure can be viewed at wileyonlinelibrary.com]

$$\frac{\partial \boldsymbol{U}}{\partial t} + \boldsymbol{U} \cdot \nabla \boldsymbol{U} = -g\nabla\zeta - \frac{1}{\rho(\overline{\zeta}+h)}[\nabla \cdot \boldsymbol{S} + \overline{\boldsymbol{\tau_b}} - \overline{\boldsymbol{\tau_s}}], \qquad (2)$$

where $\boldsymbol{S}$ is the radiation stress tensor (proportional to H^2_{rms}), $\overline{\boldsymbol{\tau_b}}$ is the mean bottom stress, and $\overline{\boldsymbol{\tau_s}}$ is the mean surface stress here approximated by a typical quadratic drag law, $\overline{\boldsymbol{\tau_s}} = \rho_a C_{Da} \boldsymbol{u}_{10}|\boldsymbol{u}_{10}|$, where air density ρ_a, wind drag coefficient C_{Da}, and wind velocity $\boldsymbol{u_{10}}$ (Smith 1988).

In December 2013, wave-driven flow through the lagoon was forced by strong northern 3-m waves (H_s) and relatively

weak southern 1-m waves (Fig. 3a). The tidally removed free surface, ζ_{dt} shows a large increase in water levels on the northern backreef (NBE), and a slight increase in the eastern lagoon (EL), compared to the channel (CHAN) (Fig. 3b). The velocity in the channel varied with the tide up to 0.38 m s^{-1} (Fig. 3c,d), with the low-pass filtered depth averaged velocity U_{Llp} directed out of the channel and largest (up to 0.2 m s^{-1}) during the period of strong waves ($H_s > 2$ m) (Fig. 3d). Thus, waves on the north of the atoll drove a net flow through the atoll system and out the main channel, a process which has been observed on other atolls (Atkinson et al. 1981; Kench 1998; Dumas et al. 2012).

The relative effect of each forcing from tides, waves, wind, and regional flow on accelerating local observed flow $\boldsymbol{U}$ in Eq. 2 is then,

$$\boldsymbol{U} \propto \boldsymbol{U}\left(\zeta_{\mathrm{OS}}, H_{\mathrm{rms}}^2, u_{10}|\boldsymbol{u}_{10}|, U_{\mathrm{reg}}\right), \tag{3}$$

where the mean tidal level ζ_{OS} was obtained from an average of all forereef sites, and filtered to retain only tidal frequencies. Coherency γ^2 (*see* Data analysis) was used to evaluate the relative importance of the forcing mechanisms in Eq. 3. Preconditioning of the $\zeta_{\mathrm{OS}}, H_{\mathrm{rms}}^2, u_{10}|\boldsymbol{u}_{10}|, U_{\mathrm{reg}}$ signals was conducted so that coherency between them was not significant. The following paragraphs each discuss the effect of forcing from tides, waves, winds, and regional flow on local observed flow.

Tides drive flow typically although large scale pressure gradients. The coherency between tidal height and observed flow was significant for all sites in both the AS and CS directions, and the maximum coherence had a period equivalent to that of the M2 or K1 tides (Fig. 4a,b). Thus, tidally driven flows were important at all measurement sites.

Waves drive flow although changes to waves from breaking and dissipation from bottom friction, which creates a force in the momentum equation from spatial gradients in radiation stress. The resulting pressure gradients drove flow onshore of the surfzone from the side of the atoll with larger waves to the side of smaller waves. This setup effect was largest when one side of the atoll has much larger waves than the other (Fig. 3). The coherency between north waves and observed flow was significant for most sites on the interior of the atoll and the channel (Fig. 4c,d) while for south waves the coherency was weakly significant on the terrace and southeast forereef (FR5) (Fig. 4e,f). The period of maximum coherency is typically hundreds of hours, reflective of the typical timescales of wave swell events from remote sources (Rogers et al. 2016). For larger waves on the north side of the atoll (which are the most common conditions), this drove flow generally from north to south through preferential pathways. Flow was enhanced through the lagoon system from east to west and flow exits through the channel (Fig. 3), confirmed through modeling results (Rogers 2015). For larger waves on the south of the atoll, this generally drove flow from south to north across the atoll; flow was not increased in the channel, as there was not a pressure gradient in that direction, but was increased across the terraces (Rogers 2015). Over the field record, waves were often larger on the north of the atoll, and thus the dominant flow path was from east to west through the lagoon system and out the channel, explaining the net long-term outflow from the channel (Supporting Information Figure SI 1b).

Winds drive flow by imparting a surface stress, which was generally weak, except likely in deeper lagoons (Lowe and Falter 2015), where no measurement stations were present. Coherency between wind and observed flow was significant only on the western terrace sites and northeast forereef (FR7) (Fig. 4g,h). Thus, wind-driven flow was generally weak at the measurement locations.

Large scale regional flows can also drive local flows. The measurement stations on the forereef (FR3, FR5, FR7, FR9) were typically within the atoll-scale turbulent boundary layer and were largely sheltered from the large-scale regional flow due to their location on the forereef (Rogers 2015). U at these sites showed no significant coherence with the large-scale flows derived from the upper 50 m of the HYCOM global model, except for one site on the forereef (FR7), which was very weak. However, in regions exposed to the regional flows such as the far eastern and western forereefs and terraces (where no observation sites existed), the regional flows can drive flow as seen in the ROMS model results (Rogers 2015).

In addition to tides, waves, winds, and regional flows driving local depth averaged flow, we also look at the relative importance of density driven flows on circulation and exchange. We approximate a two layer system, where ΔU and ΔT are the average velocity and temperature, respectively, of the upper half of the water column minus the average of the lower half (Monismith et al. 2006). The results show buoyancy driven exchange flow is important at all the forereef and channel sites, but especially in the CS direction (Fig. 4k,l). The lagoon system was stratified, and the channel velocity profile shows evidence of classic baroclinic exchange flow (Supporting Information Figure SI 2f). Additionally, surface jets of flow in the direction away from the atoll were observed in the ADCP/ADV field data at the diurnal frequency, likely from heated shallow reef flat water exiting over the reef crest (Rogers 2015). Shallow water on the reef flats was likely saltier due to differential evaporation; with cooling at night, this water could form bottom density currents that propagated into the interior lagoons or along the exterior forereefs (Gardner et al. 2011, 2014).

Thermodynamics

We now investigate the mechanism for temperature variability on a weekly timescale. Assuming depth-averaged instantaneous temperatures T, no horizontal diffusion, and no heat flux from the sea floor, the heat conservation equation is (e.g., Herdman et al. 2015),

$$\frac{\partial T}{\partial t} + \boldsymbol{U} \cdot \nabla T = \frac{H}{\rho C_p h}, \tag{4}$$

where $\boldsymbol{U}$ is depth averaged Lagrangian velocity vector, ρ is density, C_p is specific heat of water, h is depth, and H is the surface

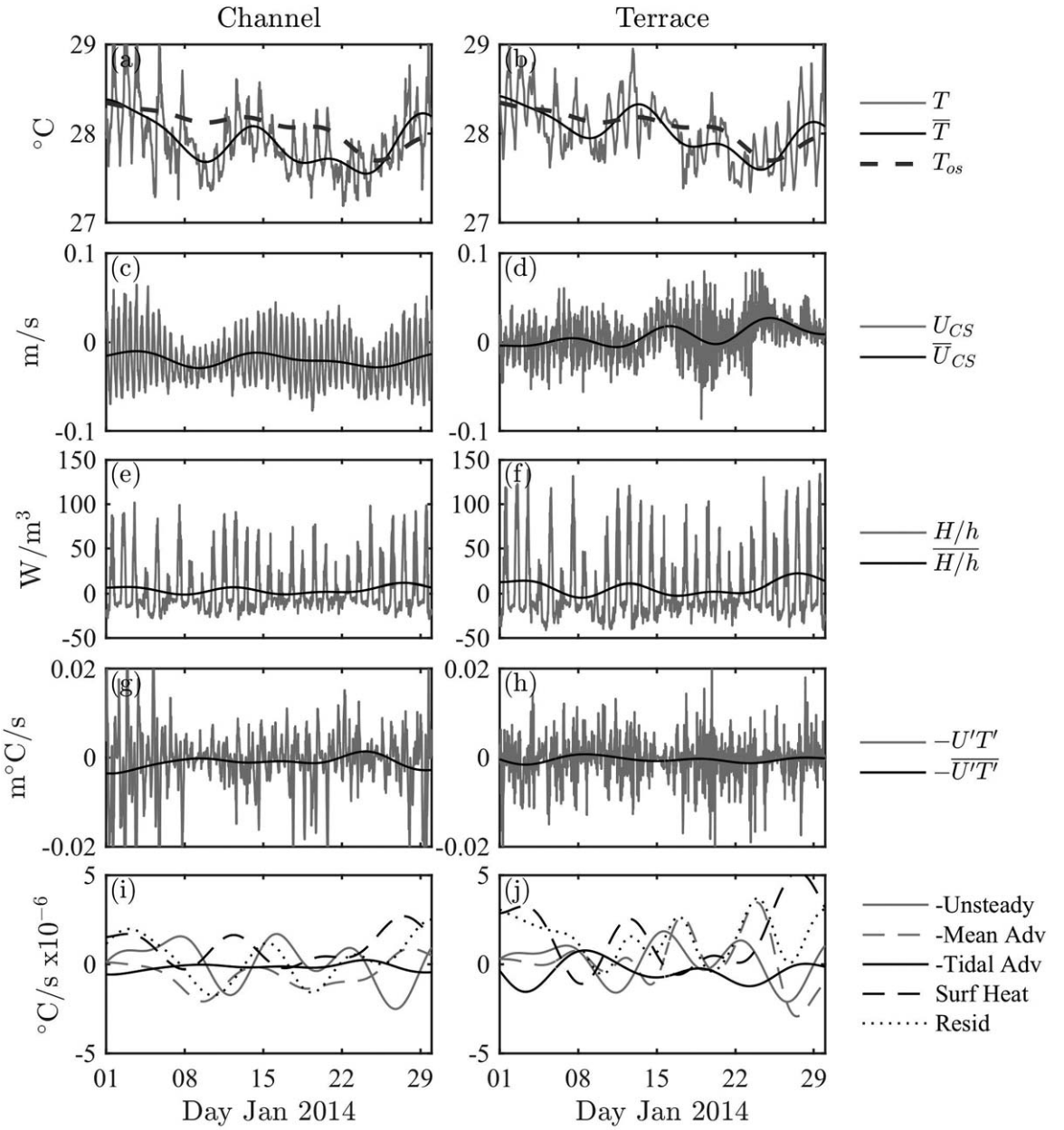

Fig. 5. Thermodynamics at Channel site (left) and Terrace RT4 site (right) in Jan 2014. (**a**,**b**) Measured instantaneous T, time averaged $\overline{T}$, and offshore average temperature T_{OS}, (**c**,**d**) measured instantaneous and time averaged cross-shore U_{CS} and time averaged velocity $\overline{U_{CS}}$, (**e**,**f**) net instantaneous H/h and average solar heat flux $\overline{H/h}$, (**g**,**h**) instantaneous $U'T'$ and average $\overline{U'T'}$ tidal transport, and (**i**,**j**) terms in heat equation (Eq. 6), shown on right-hand side, positive is heat into water column.

heat flux, the sum of shortwave radiation (H_{SW}), long wave radiation (H_{LW}), and the sensible (H_S) and latent heat (H_L) fluxes,

$$H = H_{SW} + H_{LW} + H_S + H_L, \tag{5}$$

and $H > 0$ implies heat flux into the water column. Direct measurements of long and short wave radiation along with variables necessary to estimate sensible and latent heat flux using bulk formulae (Pawlowicz et al. 2001) were made at the weather station from Sep 2013 to May 2014 (Fig. 1b). To identify weekly variability of time averaged temperature $\overline{T}$ (dropping subscript $_{7d}$), we take a 7 d time average of Eq. 4, and decompose $T = \overline{T} + T'$ and $U = \overline{U} + U'$, and assume AS temperature gradients are weak,

$$\frac{\partial \overline{T}}{\partial t} + \overline{U}\frac{\partial \overline{T}}{\partial x} + \overline{U'\frac{\partial T'}{\partial x}} = \overline{\frac{H}{\rho C_p h}}, \tag{6}$$

where the terms from left to right will be referred to as unsteady, mean advection, tidal advection, and surface

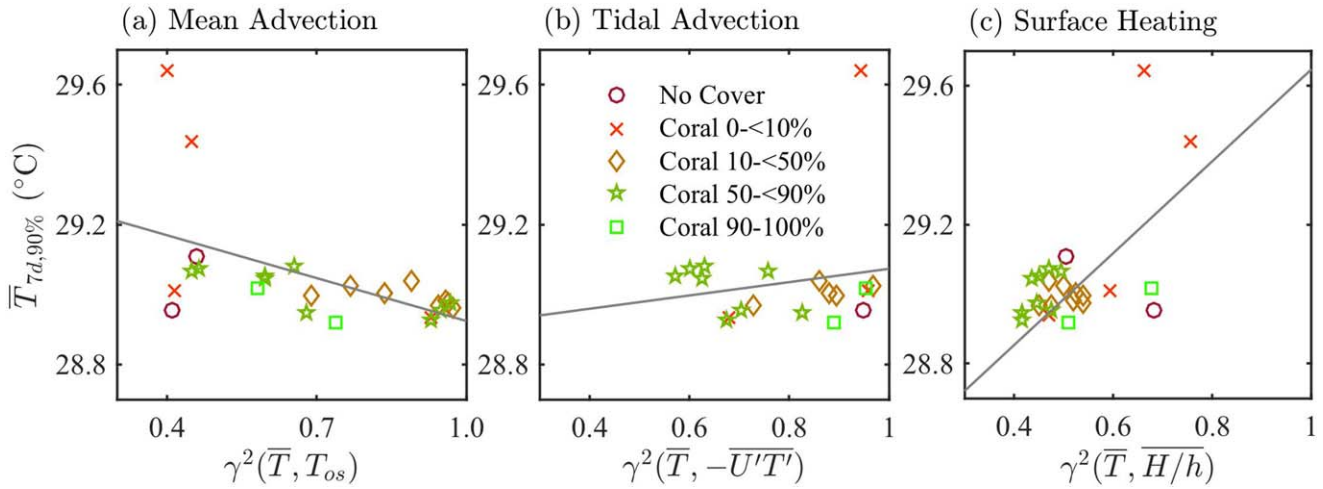

Fig. 6. Effect of mean advection, tidal advection, and surface heating in driving high mean weekly temperatures at sites with different biological cover. Maximum coherency γ^2 of $\overline{T}$ with (**a**) mean advection T_{os}, (**b**) tidal advection $-\overline{U'T'}$, and (**c**) surface heating $\overline{H/h}$, as a function of high weekly temperature $\overline{T}_{7d,90\%}$. Solid gray line is best fit to data, and 95% significant coherency is 0.22. Analysis is for September 2013 to April 2014. [Color figure can be viewed at wileyonlinelibrary.com]

heating. We evaluate Eq. 6 at the midpoint between each site in Fig. 1b and offshore. We approximate $\partial\overline{T} \approx \overline{T} - T_{OS}$, and $\partial T' \approx T'$ (as $T'_{OS}=0$). Furthermore, U in Eq. 6 was taken as a fraction α times the CS velocity measured at each site to reflect the average CS velocity between offshore (which is near 0) and the measurement location; α can vary between 0 and 1 and was taken as value to minimize the least squares error in Eq. 6 (e.g. α was 0.2 and 0.5 for CHAN and RT4 sites, respectively).

To illustrate Eq. 6 in two different regimes, we present the thermodynamics at the Channel (CHAN) and Terrace (RT4) sites during January 2014, noting that while diurnal temperature variations were about 1°C, mean temperatures $\overline{T}$ were within ± 0.2°C of the offshore temperature T_{OS} (Fig. 5a,b). Cross shore velocity at the channel site had strong tidal variability (± 0.05 m s^{-1}) with a net negative mean, while at the terrace site, variability was generally smaller (± 0.03 m s^{-1}) with a mean fluctuating about zero (Fig. 5c,d). Local heating was diurnal, inversely proportional to depth, and positive on average (heat flux into water column) and was weaker at the deeper Channel site (−20 W m^{-3} to 100 W m^{-3}) than the shallower Terrace site (−30 W m^{-3} to 150 W m^{-3}) (Fig. 5e,f). The tidal transport of temperature $-U'T'$ results from the correlation of temperature deviations (primarily diurnal) and velocity deviations (primarily M2/K1 tidal). The average $-\overline{U'T'}$ transports heat depending on the relative phase of temperature and velocity and was net negative at the channel site (net export of heat) and near zero at the terrace site (Fig. 5g,h). The resulting heat balance shows that at both sites, while tidal advection was the smallest term, all terms were important (> 10% total) (Fig. 5i,j). Note that while the heat budget does not close exactly, the residual error is of the same order as the terms.

The mean advection term should be proportional to T_{OS} when $\overline{U}$ is significant, and thus $\overline{U}\frac{\partial\overline{T}}{\partial x} \propto T_{OS}$. This is confirmed by comparing T_{OS} (Fig. 5a,b) to the computed mean advective term (Fig. 5i,j). To evaluate the tidal advective term, assuming $\partial T' \approx T' - T'_{OS} = T'$, and thus $\overline{U'\frac{\partial T'}{\partial x}} \propto \overline{U'T'}$. This is confirmed by comparing $-\overline{U'T'}$ (Fig. 5g,h) to the computed tidal advective term (Fig. 5i,j). For sites where velocity measurements were not available, U' was assumed the same as nearby gauges in similar regimes (i.e., RT4 is similar to RT1). For sites where no nearby observations existed, (all shallow backreef sites), a least squares regression was performed using the ROMS simulations (Rogers 2015), at each site assuming U' was primarily tidally driven by pressure gradients. The relative effect of each forcing on $\overline{T}$ from mean advection, tidal advection, and surface heating in Eq. 6 is then,

$$\overline{T} \propto \overline{T}\left(T_{OS}, -\overline{U'T'}, \overline{H/h}\right). \quad (7)$$

To statistically evaluate the importance of different terms in Eq. 7 on forcing weekly temperature variability at all the sites, we used coherency γ^2 between $\overline{T}$ and each term in Eq. 6. Each of the three terms on the right side of Eq. 7 was prefiltered so that they were not coherent with each other.

The results of the coherency analysis of Eq. 7 are shown in Fig. 6, with maximum coherency from the spectra reported. High weekly temperature $\overline{T}_{7d,90\%}$ generally increased with decreased mean advection ($R^2 = 0.30$, $p = 0.005$) (Fig. 6a), did not significantly increase with increased tidal advection ($R^2 = 0.03$, $p = 0.49$) (Fig. 6b), and generally increased with increased surface heating ($R^2 = 0.30$, $p = 0.05$) (Fig. 6c).

Coral cover

The results of the coherency analysis of temperature showed that sites with live coral cover (> 10%) were generally associated with higher mean advection, lower tidal advection, and lower surface heating compared to sites with low (< 10%)

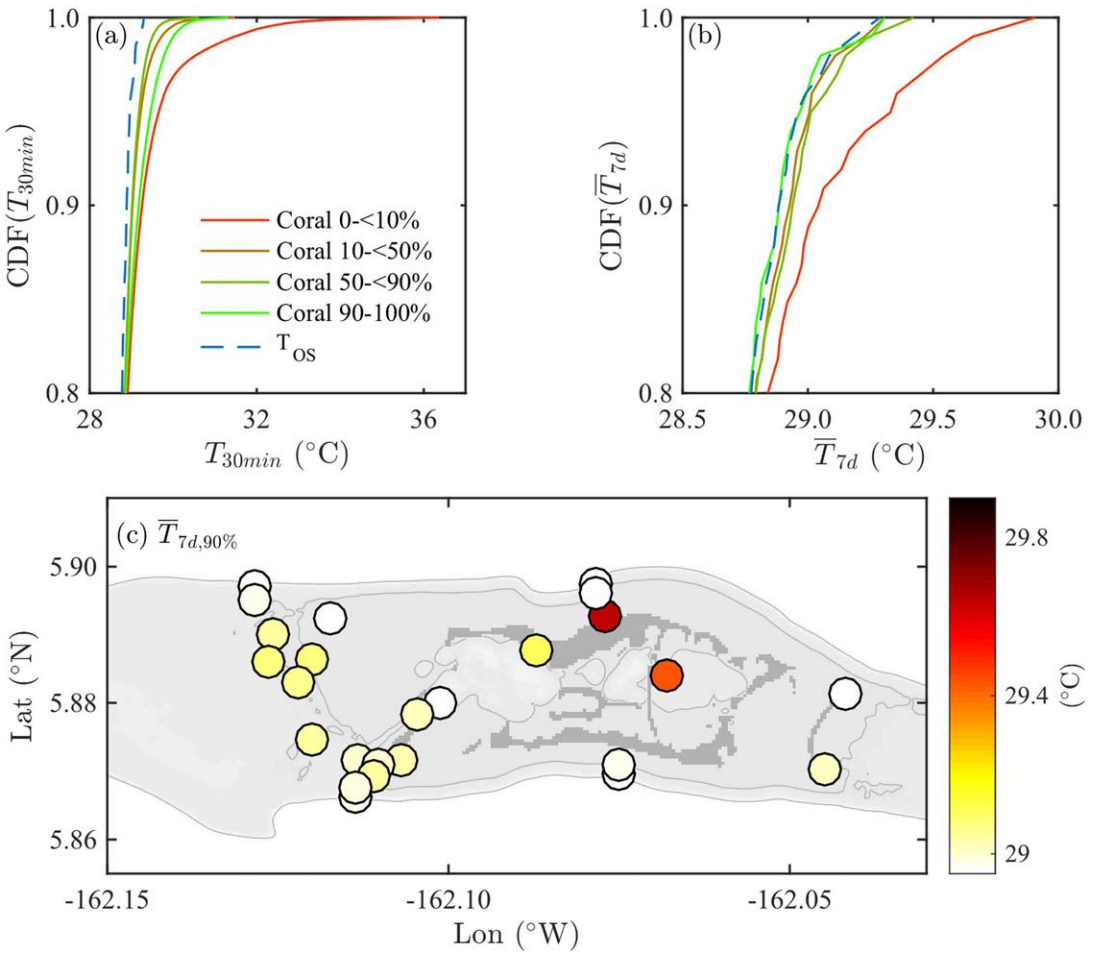

Fig. 7. Temperature statistics. Cumulative probability (CDF) of temperature at sites with varying coral cover compared to offshore T_{OS}, with (**a**) measured 30-min data $\overline{T}_{30min}$, and (**b**) 7-d time average $\overline{T}_{7d}$; and (**c**) spatial distribution of average of top 90% of weekly average temperatures $\overline{T}_{7d,90}$%. Results are over all available data from 2012 to 2014, note only high cumulative probability shown (0.8–1) for (a) and (b).

to no cover (Fig. 6). We further examined the long-term temperature dynamics at a time scale relevant to corals on the reef using the multi-year field records. The cumulative probability of measured temperature T_{30min} showed a highly variable distribution when combining temperature records for similar coral cover types. The combined temperature distribution of sites of low (< 10%) and high (> 90%) coral cover experienced temperatures up to 36°C and 31.5°C, respectively, both of which were higher than offshore (Fig. 7a). The offshore temperature T_{OS} was computed as the mean of all fore-reef sites after applying a 7-d low-pass filter to remove variability from diurnal effects and internal waves.

Sites with moderate or high coral cover (> 10%) had generally lower weekly averaged temperatures ($\overline{T}_{7d}$) relative to other sites across the atoll and that were similar to T_{OS}, while sites with low coral cover (< 10%) experienced significantly higher temperatures (up to 0.6°C) than offshore (Fig. 7b, confirmed using a Kolmogorov–Smirnov test of the distributions). The median temperature (0.5 probability) was similar for all sites at both time scales (not shown). Thus, although sites of different benthic cover types generally exhibited similar diurnal temperature variability, average weekly temperatures in sites with moderate or high live coral cover were similar to offshore waters and lower than sites with little to no live coral. The spatial distribution of mean of the top 90% of the weekly averaged temperature $\overline{T}_{7d,90}$%, shows how sites which were more open and/or closer to offshore waters exhibited lower weekly temperatures than sites that were more closed and/or more remote relative to offshore waters (Fig. 7c).

Travel time results from the 100 m bathymetric contour to a point within the atoll interior were taken from ROMS model results using Lagrangian passive tracers (Rogers 2015). Sites in the backreef with low coral cover were strongly associated with high temperatures, while sites in the lagoons with low- to no coral cover were associated with high temperatures and/or high travel time (Fig. 8a). Wave stress results were taken from the SWAN model, using the 95th percentile of bottom velocity squared as a proxy for bottom

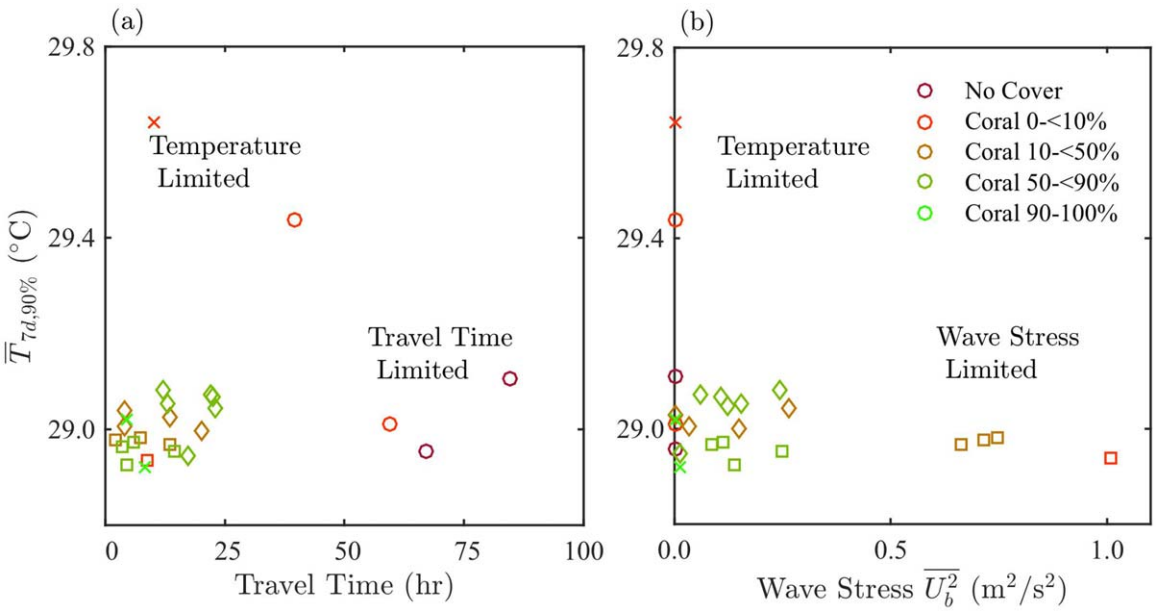

Fig. 8. Variation in percent coral cover with limiting physical dynamics, (**a**) high weekly temperature $\overline{T}_{7d,90\%}$, with travel time from offshore, (**b**) $\overline{T}_{7d,90\%}$ with wave bottom stress proxy $\overline{U_b^2}$, categorized by hydrodynamic regime. Color denotes coral cover, symbol denotes regime: o is lagoon, x is back reef, ◇ is terrace, and □ is forereef.

stress (Rogers et al. 2016). Wave stress showed a strong control over coral cover on the forereef, with locations of very high stress associated with lower coral cover (Fig. 8b).

Discussion

Hydrodynamics and thermodynamics

The wave driven flow was typically forced by waves from the north, which created an elevated free surface on the north shallow backreef, and drove a mean circulation through the atoll lagoon system (Fig. 9). Seasonal increases in MSL (±0.2 m) (Fig. 2b) likely increased this wave driven flow, especially over the shallow reef crest (Monismith 2007). The thermodynamics at the weekly timescale were controlled by mean advection, tidal advection and surface heating. At this timescale, increased advection from wave-forced mean flows typically lowered temperatures because of the increased connectivity with offshore waters. Tidal advection transported heat when tidal flow and diurnal heating were in phase, but did not significantly affect the weekly temperatures on the atoll. Surface heating increased temperatures and is primarily a function of depth. Overall, mean advection and surface heating were the primary controls on weekly temperature variations on the atoll.

The results from this study are likely extendible to other atolls that are also wave or tidally dominated (i.e., most reefs globally; Lowe and Falter 2015) and have temperatures near the thermal limit of corals inhabiting them (i.e., most shallow reefs; Hoegh-Guldberg et al. 2007; Carpenter et al. 2008). The results obtained from specific areas of Palmyra Atoll are also likely extensible to other similar reef systems regardless of whether they are part of a larger atoll. For example, the hydrodynamics and thermodynamics we observed on the submerged east and west terraces of Palmyra are similar to those observed on platform and barrier reefs [e.g., Red Sea platform, (Davis et al. 2011)]. A similar analogy could be drawn between the forereef and shallow backreef areas on Palmyra with fringing reefs studied elsewhere in the Indo-Pacific [e.g., Moorea, (Herdman et al. 2015)]. However, to our knowledge no similar studies exist on other reefs to mechanistically explain observed weekly temperature variations and how they may be influencing spatial variation in coral cover, a topic which should be applied in other field sites.

Ecological implications

Although temperatures at all sites across Palmyra exhibited variation on multiple time scales, the timescale most relevant to explaining spatial variations in coral cover across Palmyra is over several days to weeks. Interestingly, degree heating week, a common measure of large scale thermal stress uses a 12-week window (Strong et al. 2011), but the results from this study and others suggest a shorter window may be more appropriate to match the incidence of coral bleaching with the onset of ocean warming events (Goreau and Hayes 1994; Reaser et al. 2000). While numerous physical factors can influence coral cover, sites with moderate to high coral cover (> 10%) were generally associated with lower weekly temperatures that were similar to offshore

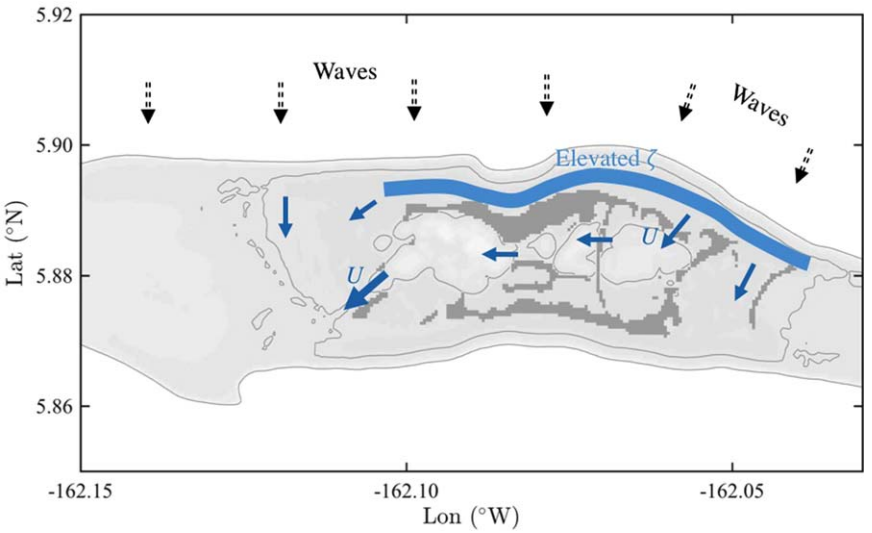

Fig. 9. Typical wave-driven circulation on atoll at a subtidal timescale. Strong wave forcing from the north (black) creates elevated free surface ζ on the north shallow backreef (blue), driving a mean circulation U through the atoll lagoon system (dark blue). Light gray lines are 5- and 60-m depth contours, and light gray shading is land. [Color figure can be viewed at wileyonlinelibrary.com]

waters, while sites with low coral cover or no cover (< 10%) were generally associated with high weekly temperatures.

Because of the vibrant coral reef ecosystem on the atoll's terraces and forereefs (Williams et al. 2013), the spatial variation in thermal and hydrodynamic properties is of particular ecological relevance. While the sites with high coral cover were generally associated with lower temperatures, some notable exceptions exist (Fig. 8). Coral growth can be affected by high temperatures, but it can also be affected by other physical factors such as wave stress, light penetration, travel time/residence time, sediment, and so forth. (Chappell 1980). On Palmyra, light was generally not limiting at depths less than 30 m (Williams et al. 2013; Rogers et al. 2016), and suspended sediment is typically not significant on the atoll given its size and exposure to the open ocean.

Travel time for a parcel of water moving from a boundary to some point within a region is often termed "water age" (Monsen et al. 2002; Rayson et al. 2016). For tropical atolls with open platforms, the relevant boundary is the atoll exterior (taken as 100-m depth), and travel time is thus a measure of the atoll influence on the offshore waters for quantities such as temperature and nutrients. Travel time is also relevant to reefs since it essentially asks how long a parcel of water has been in the atoll system before it gets to a certain point, instead of how long it takes to exit the system after leaving a certain point (residence time).

Sites in the backreef with low coral cover were strongly associated with high temperatures while sites in the lagoons with low- to no coral cover were associated with high temperatures and/or high travel time. Areas within the terrace and forereef were all associated with low temperature and shorter travel times. The backreef and lagoon sites associated with high temperature are sites with very shallow depth (< 1 m), low net exchange, and long distance from the reef crest and thus highly sensitive to the effects of local heating. The lagoon areas associated with long travel time and low temperature were likely negatively impacted by poor water quality. While the exact mechanism of this effect on corals is not known, the lagoon bottom waters are known to be anoxic and sulfidic and thus prohibit coral growth (Gardner et al. 2014). Prior to extensive development of the atoll lagoon areas during WWII which severely restricted lagoon flows, the interior lagoons contained vibrant reefs (Collen et al. 2009).

Waves are another important mechanism which can modify the reef, and wave induced stress has been shown to be significantly correlated with coral cover on Palmyra (Rogers et al. 2016). Modeled wave stress showed a strong control over coral cover on the forereef, with locations of very high stress associated with lower coral cover.

Conclusions

The results of our study suggest that temperature, travel time, and wave stress likely have a strong influence on the distribution of coral cover across Palmyra. However, our results should be interpreted within a broader range of ecological factors affecting the growth and distribution of coral across Palmyra. With future climate change, net warming of waters could push all of these regimes to higher temperatures increasing the risk for mortality. Indeed, mild bleaching was observed at many locations on the atoll during the 2008 El Niño event when monthly mean temperatures ranged from 29.8°C to 30.1°C (Williams et al. 2010), and preliminary observations from the 2015 to 2016 El Niño event

indicate bleaching on the atoll (B. Zgliczynski, personal comm.). Based on our results, we believe the sites which have the best likelihood of survival through lower temperatures and shorter offshore travel time are associated with high mean advection, typically the result of wave-driven flow or oceanic conditions with high-exchange. At shallow depths, this trend would likely be enhanced with increased depth from sea level rise increasing wave driven flow over the reef crest. While tides were also important in driving flow on the atoll, their contribution to the net transport of heat was not significant. The results from this study are likely extendible to other atolls which are also wave or tidally dominated (most reefs globally) and also have temperatures near the thermal limit of corals inhabiting them (most shallow reefs globally). Future work could further examine the effects of density-driven flow in atoll systems, especially focusing on the interior lagoons. Additionally, future work should aim to couple high resolution ecological and temperature studies to better understand biophysical coupling on coral reefs.

References

Andréfouët, S., and others. 2006. Review of solutions for 3D hydrodynamic modeling applied to aquaculture in South Pacific atoll lagoons. Mar. Pollut. Bull. **52**: 1138–1155. doi:10.1016/j.marpolbul.2006.07.014

Andrews, D. G., and M. E. Mcintyre. 1978. An exact theory of nonlinear waves on a Lagrangian-mean flow. J. Fluid Mech. **89**: 609. doi:10.1017/S0022112078002773

Arístegui, J., P. Sangrá, S. Hernández-León, M. Cantón, A. Hernández-Guerra, and J. L. Kerling. 1994. Island-induced eddies in the Canary Islands. Deep Sea Res. Part I Oceanogr. Res. Pap. **41**: 1509–1525. doi:10.1016/0967-0637(94)90058-2

Atkinson, M. J., S. V. Smith, and E. D. Stroup. 1981. Circulation in Enewetak Atoll lagoon. Limnol. Oceanogr. **26**: 1074–1083. doi:10.4319/lo.1981.26.6.1074

Bruno, J. F., and others. 2007. Thermal stress and coral cover as drivers of coral disease outbreaks. PLoS Biol. **5**: 1220–1227. doi:10.1371/journal.pbio.0050124

Callaghan, D. P., P. Nielsen, N. Cartwright, M. R. Gourlay, and T. E. Baldock. 2006. Atoll lagoon flushing forced by waves. Coast. Eng. **53**: 691–704. doi:10.1016/j.coastaleng.2006.02.006

Carpenter, K. E., and others. 2008. One-third of reef-building corals face elevated extinction risk from climate change and local impacts. Science **321**: 560–563. doi:10.1126/science.1159196

Chappell, J. 1980. Coral morphology, diversity and reef growth. Nature **286**: 249–252. doi:10.1038/286249a0

Collen, J. D., D. W. Garton, and J. P. A. Gardner. 2009. Shoreline changes and sediment redistribution at Palmyra Atoll (Equatorial Pacific Ocean): 1874–Present. J. Coast. Res. **253**: 711–722. doi:10.2112/08-1007.1

Dandan, S. S., J. L. Falter, R. J. Lowe, and M. T. McCulloch. 2015. Resilience of coral calcification to extreme temperature variations in the Kimberley region, northwest Australia. Coral Reefs **34**: 1151–1163. doi:10.1007/s00338-015-1335-6

Davis, K. A., S. J. Lentz, J. Pineda, J. T. Farrar, V. R. Starczak, and J. H. Churchill. 2011. Observations of the thermal environment on Red Sea platform reefs: A heat budget analysis. Coral Reefs **30**: 25–36. doi:10.1007/s00338-011-0740-8

Dean, R. G., and R. A. Dalrymple. 1991. Water wave mechanics for engineers and scientists. World Scientific Publishing Co. Inc.

Delesalle, B., and A. Sournia. 1992. Residence time of water and phytoplankton biomass in coral reef lagoons. Cont. Shelf Res. **12**: 939–949. doi:10.1016/0278-4343(92)90053-M

Douillet, P., S. Ouillon, and E. Cordier. 2001. A numerical model for fine suspended sediment transport in the southwest lagoon of New Caledonia. Coral Reefs **20**: 361–372. doi:10.1007/s00338-001-0193-6

Dumas, F., R. Le Gendre, Y. Thomas, and S. Andréfouët. 2012. Tidal flushing and wind driven circulation of Ahe atoll lagoon (Tuamotu Archipelago, French Polynesia) from in situ observations and numerical modelling. Mar. Pollut. Bull. **65**: 425–440. doi:10.1016/j.marpolbul.2012.05.041

Emery, W. J., and R. E. Thomson. 2004. Data analysis methods in physical oceanography, 2nd ed. Elsevier.

Gardner, J. P. A., D. W. Garton, and J. D. Collen. 2011. Near-surface mixing and pronounced deep-water stratification in a compartmentalised, human-disturbed atoll lagoon system. Coral Reefs **30**: 271–282. doi:10.1007/s00338-010-0701-7

Gardner, J. P. A., D. W. Garton, J. D. Collen, and D. Zwartz. 2014. Distant storms as drivers of environmental change at Pacific atolls. PLoS One **9**: e87971. doi:10.1371/journal.pone.0087971

Goreau, T., and R. Hayes. 1994. Coral bleaching and ocean "hot spots." AMBIO **23**: 176–180. doi:10.1371/journal.pone.0087971

Gove, J., G. Williams, M. McManus, S. Clark, J. Ehses, and L. Wedding. 2015. Coral reef benthic regimes exhibit nonlinear threshold responses to natural physical drivers. Mar. Ecol. Prog. Ser. **522**: 33–48. doi:10.3354/meps11118

Herdman, L. M. M., J. L. Hench, and S. G. Monismith. 2015. Heat balances and thermally driven lagoon-ocean exchangeson a tropical coral reef system(Moorea, French Polynesia). J. Geophys. Res. Ocean. **120**: 1233–1252. doi:10.1002/2014JC010145

Hoegh-Guldberg, O., and others. 2007. Coral reefs under rapid climate change and ocean acidification. Science **318**: 1737–1742. doi:10.1126/science.1152509

Hoeke, R. K., C. D. Storlazzi, and P. V. Ridd. 2013. Drivers of circulation in a fringing coral reef embayment: A wave-flow coupled numerical modeling study of Hanalei Bay,

Hawaii. Cont. Shelf Res. **58**: 79–95. doi:10.1016/j.csr.2013.03.007

Hsin, Y. C. C., and B. Qiu. 2012. Seasonal fluctuations of the surface North Equatorial Countercurrent (NECC) across the Pacific basin. J. Geophys. Res. Ocean **117**: 1–17: doi:10.1029/2011JC007794

Hughes, T. P., and others. 2003. Climate change, human impacts, and the resilience of coral reefs. Science **301**: 929–933. doi:10.1126/science.1085046

Kench, P. S. 1998. Physical processes in an Indian Ocean atoll. Coral Reefs **17**: 155–168. doi:10.1007/s003380050110

Koweek, D. A., R. B. Dunbar, J. S. Rogers, G. J. Williams, N. Price, D. A. Mucciarone, and L. Teneva. 2015. Environmental and ecological controls of coral community metabolism on Palmyra Atoll. Coral Reefs **34**: 339–351. doi:10.1007/s00338-014-1217-3

Kraines, S., T. Yanagi, M. Isobe, and H. Komiyama. 1998. Wind-wave driven circulation on the coral reef at Bora Bay, Miyako Island. Coral Reefs **17**: 133–143. doi:10.1007/s003380050107

Lentz, S. J., J. H. Churchill, K. A. Davis, J. T. Farrar, J. Pineda, and V. Starczak. 2016. The characteristics and dynamics of wave-driven flow across a platform coral reef in the Red Sea. J. Geophys. Res. Ocean **121**: 1360–1376. doi:10.1002/2015JC011141

Longuet-Higgins, M. S., and R. W. Stewart. 1964. Radiation stresses in water waves; a physical discussion, with applications. Deep Sea Res. Oceanogr. Abstr. **11**: 529–562. doi:10.1016/0011-7471(64)90001-4

Lowe, R. J., and J. L. Falter. 2015. Oceanic Forcing of Coral Reefs. Ann. Rev. Mar. Sci. **7**: 43–66. doi:10.1146/annurev-marine-010814-015834

Lowe, R. J., J. L. Falter, S. G. Monismith, and M. J. Atkinson. 2009. A numerical study of circulation in a coastal reef-lagoon system. J. Geophys. Res. Ocean **114**: 1–18. doi:10.1029/2008JC005081

Lugo-Fernández, A., H. H. Roberts, and W. J. Wiseman. 2004. Currents, water levels, and mass transport over a modern Caribbean coral reef: Tague Reef, St. Croix, USVI. Cont. Shelf Res. **24**: 1989–2009. doi:10.1016/j.csr.2004.07.004

Maragos, J., J. Miller, J. Gove, and E. Demartini. 2008. US coral reefs in the Line and Phoenix Islands, Central Pacific Ocean 1: History, geology, oceanography, and biology. Coral Reefs USA **1**: 595–641. doi:10.1007/978-1-4020-6847-8_15

Mayfield, A. B., M. N. Chen, P. J. Meng, H. J. Lin, C. S. Chen, and P. J. Liu. 2013. The physiological response of the reef coral Pocillopora damicornis to elevated temperature: Results from coral reef mesocosm experiments in Southern Taiwan. Mar. Environ. Res. **86**: 1–11. doi:10.1016/j.marenvres.2013.01.004

Mei, C., M. Stiassnie, and D. Yue. 2005. Theory and applications of ocean surface waves, World Scientific Publishing Co. Inc.

Monismith, S. G. 2007. Hydrodynamics of Coral Reefs. Annu. Rev. Fluid Mech. **39**: 37–55. doi:10.1146/annurev.fluid.38.050304.092125

Monismith, S. G., A. Genin, M. A. Reidenbach, G. Yahel, and J. R. Koseff. 2006. Thermally Driven Exchanges between a Coral Reef and the Adjoining Ocean. J. Phys. Oceanogr. **36**: 1332–1347. doi:10.1175/JPO2916.1

Monismith, S. G., J. S. Rogers, D. A. Koweek, and R. B. Dunbar. 2015. Frictional wave dissipation on a remarkably rough reef. Geophys. Res. Lett. **42**: 1–9. doi:10.1002/2015GL063804

Monsen, N. E., J. E. Cloern, L. V. Lucas, and S. G. Monismith. 2002. The use of flushing time, residence time, and age as transport time scales. Limnol. Oceanogr. **47**: 1545–1553. doi:10.4319/lo.2002.47.5.1545

Munk, W. H., and M. C. Sargent. 1948. Adjustment of Bikini Atoll to ocean waves. Trans. Am. Geophys. Union **29**: 855. doi:10.1029/TR029i006p00855

Palumbi, S. R., D. J. Barshis, N. Traylor-Knowles, and R. A. Bay. 2014. Mechanisms of reef coral resistance to future climate change. Science **344**: 895–898. doi:10.1126/science.1251336

Pawlowicz, R., B. Beardsley, S. Lentz, E. Dever, and A. Anis. 2001. Software simplifies air-sea data estimates. Eos, Trans. Am. Geophys. Union **82**: 2. doi:10.1029/01EO00004

Rayson, M. D., E. S. Gross, R. D. Hetland, and O. B. Fringer. 2016. Time scales in Galveston Bay: An unsteady estuary. J. Geophys. Res. Oceans **121**: 2268–2285. doi:10.1002/2015JC011181

Reaser, J. K., R. Pomerance, and P. O. Thomas. 2000. Coral bleaching and global climate change: Scientific findings and policy recommendations. Conserv. Biol. **14**: 1500–1511. doi:10.1046/j.1523-1739.2000.99145.x

Riegl, B., and R. Dodge. 2008. Coral reefs of the USA. Elsevier.

Rogers, J. S. 2015. Physical oceanography in coral reef environments wave and mean flow dynamics at small and large scales, and resulting ecological implications. Stanford University.

Rogers, J. S., S. G. Monismith, R. B. Dunbar, and D. A. Koweek. 2015. Field observations of wave-driven circulation over spur and groove formations on a coral reef. J. Geophys. Res. **120**: 145–160. doi:10.1002/2014JC010464

Rogers, J. S., S. G. Monismith, D. A. Koweek, and R. B. Dunbar. 2016. Wave dynamics of a Pacific Atoll with high frictional effects. J. Geophys. Res. **121**: 350–367. doi:10.1002/2015JC011170

Rosman, J. H., and J. L. Hench. 2011. A framework for understanding drag parameterizations for coral reefs. J. Geophys. Res. Ocean **116**: 1–15. doi:10.1029/2010JC006892

Sandin, S. A., and others. 2008. Baselines and degradation of coral reefs in the Northern Line Islands. PLoS One **3**: e1548. doi:10.1371/journal.pone.0001548

Smith, N. P. 2001. Weather and hydrographic conditions associated with coral bleaching: Lee Stocking Island, Bahamas. Coral Reefs **20**: 415–422. doi:10.1007/s00338-001-0189-2

Smith, S. D. 1988. Coefficients for sea surface wind stress, heat flux, and wind profiles as a function of wind speed and temperature. J. Geophys. Res. **93**: 15467–15472. doi:10.1029/JC095iC02p01777

Stevenson, C., and others. 2007. High apex predator biomass on remote Pacific islands. Coral Reefs **26**: 47–51. doi:10.1007/s00338-006-0158-x

Stevenson, S., B. S. Powell, M. A. Merrifield, K. M. Cobb, J. Nusbaumer, and D. Noone. 2015. Characterizing seawater oxygen isotopic variability in a regional ocean modeling framework: Implications for coral proxy records. Paleoceanography **30**: 1573–1593. doi:10.1002/2015PA002824

Strong, A. E., G. Liu, W. Skirving, and C. M. Eakin. 2011. NOAA's coral reef watch program from satellite observations. Ann. GIS **17**: 83–92. doi:10.1080/19475683.2011.576266

Symonds, G., K. P. Black, and I. R. Young. 1995. Wave-driven flow over shallow reefs. J. Geophys. Res. **100**: 2639. doi:10.1029/94JC02736

Warner, J. C., B. Armstrong, R. He, and J. B. Zambon. 2010. Development of a Coupled Ocean–Atmosphere–Wave–Sediment Transport (COAWST) modeling system. Ocean Model. **35**: 230–244. doi:10.1016/j.ocemod.2010.07.010

Wells, J. R., J. P. Fram, and G. Pawlak. 2012. Solar warming of near-bottom water over a fringing reef. J. Mar. Res. **70**: 641–660. doi:10.1357/002224012805262734

Williams, G. J., I. S. Knapp, J. E. Maragos, and S. K. Davy. 2010. Modeling patterns of coral bleaching at a remote Central Pacific atoll. Mar. Pollut. Bull. **60**: 1467–1476. doi:10.1016/j.marpolbul.2010.05.009

Williams, G. J., J. E. Smith, E. J. Conklin, J. M. Gove, E. Sala, and S. A. Sandin. 2013. Benthic communities at two remote Pacific coral reefs: Effects of reef habitat, depth, and wave energy gradients on spatial patterns. PeerJ. **1**: e81. doi:10.7717/peerj.81

Wolanski, E., T. Asaeda, A. Tanaka, and E. Deleersnijder. 1996. Three-dimensional island wakes in the field, laboratory experiments and numerical models. Cont. Shelf Res. **16**: 1437–1452. doi:10.1016/0278-4343(95)00087-9

Young, I. R. 1989. Wave transformation over coral reefs. J. Geophys. Res. **94**: 9779. doi:10.1029/JC094iC07p09779

Zhang, Z., J. Falter, R. Lowe, G. Ivey, and M. McCulloch. 2013. Atmospheric forcing intensifies the effects of regional ocean warming on reef-scale temperature anomalies during a coral bleaching event. J. Geophys. Res. Ocean **118**: 4600–4616. doi:10.1002/jgrc.20338

Acknowledgments

The authors wish to acknowledge the field team: Mallory Barkdull, Ron Harrell, Joel Leavitt, Hank Lynch, David Mucciarone, Lida Teneva, and Gareth Williams. Editing by the Associate Editor Jim Falter and two anonymous reviewers significantly improved the manuscript. Bathymetry and other information were provided by Jamison Gove. Research funding was provided by Stanford University along with two grants from the Gordon and Betty Moore Foundation ("Observations and modeling of the C system dynamics at Palmyra Atoll: In support of the development of management strategies for ocean acidification impacts in the tropics," to RBD and, "Understanding coral reef resilience to advance science and conservation," to RBD and SGM), as well as a grant from the National Science Foundation OCE-1536502 ("Collaborative Research: Wave driven flow through a shallow, fringing reef" to SGM). This research was made with Government support under and awarded by the U.S. Department of Defense, Office of Naval Research, National Defense Science and Engineering Graduate (NDSEG) Fellowship, 32 CFR 168a to JSR. DAK was funded by an National Science Foundation Graduate Research Fellowship (DGE-114747). This is Palmyra Atoll Research Consortium contribution number PARC-124.

Conflict of Interest

None declared.

Submitted 10 February 2016
Revised 10 May 2016; 1 June 2016
Accepted 13 June 2016

Associate editor: James Falter